

A modified lognormal approximation of the Lyman- α forest: comparison with full hydrodynamic simulations at $2 \leq z \leq 2.7$

B. Arya,^{a,1} T. Roy Choudhury,^b A. Paranjape.^a and P. Gaikwad^c

^aInter-University Centre for Astronomy & Astrophysics,
Ganeshkhind, Post Bag 4, Pune 411007, India

^bNational Centre for Radio Astrophysics, TIFR,
Post Bag 3, Ganeshkhind, Pune 411007, India

^cMax-Planck-Institut für Astronomie,
Königstuhl 17, D-69117 Heidelberg, Germany
E-mail: bharya@iucaa.in, tirth@ncra.tifr.res.in, aseem@iucaa.in,
gaikwad@mpia-hd.mpg.de

Abstract. Observations of the Lyman- α forest in distant quasar spectra with upcoming surveys are expected to provide significantly larger and higher-quality datasets. To interpret these datasets, it is imperative to develop efficient simulations. One such approach is based on the assumption that baryonic densities in the intergalactic medium (IGM) follow a lognormal distribution. We extend our earlier work to assess the robustness of the lognormal model of the Lyman- α forest in recovering the parameters characterizing IGM state, namely, the mean-density IGM temperature (T_0), the slope of the temperature-density relation (γ), and the hydrogen photoionization rate (Γ_{12}), by comparing with high-resolution Sherwood SPH simulations across the redshift range $2 \leq z \leq 2.7$. These parameters are estimated through a Markov Chain Monte Carlo (MCMC) technique, using the mean and power spectrum of the transmitted flux. We find that the usual lognormal distribution of IGM densities cannot recover the parameters of the SPH simulations. This limitation arises from the fact that the SPH baryonic density distribution cannot be described by a simple lognormal form. To address this, we extend the model by scaling the linear density contrast by a parameter ν . While the resulting baryonic density is still lognormal, the additional parameter gives us extra freedom in setting the variance of density fluctuations. With this extension, values of T_0 and γ implied in the SPH simulations are recovered at $\sim 1 - \sigma$ ($\lesssim 10\%$) of the median (best-fit) values for most redshifts bins. However, this extended lognormal model cannot recover Γ_{12} reliably, with the best-fit value discrepant by $\gtrsim 3 - \sigma$ for $z > 2.2$. Despite this limitation in the recovery of Γ_{12} , whose origins we explain, we argue that the model remains useful for constraining cosmological parameters.

Keywords: intergalactic media, Lyman- α forest, power spectrum

¹Corresponding author.

Contents

1	Introduction	1
2	Simulations & Method	2
2.1	Lognormal approximation	2
2.2	SPH simulation	4
2.3	Skewer configuration and covariance matrices	4
3	Results	5
3.1	2-parameter fit	5
3.2	5-parameter fit	8
4	Discussion	11
4.1	Recovery of Γ_{12}	11
4.2	Potential application	13
4.3	Comparison with other methods	14
5	Conclusions	15

1 Introduction

The Lyman- α ($\text{Ly}\alpha$) forest observed in the spectra of distant quasi-stellar objects (QSOs) is a useful tracer for probing the underlying cosmic density field at relatively small scales [1–4]. The properties of the forest are sensitive to the thermal and ionization state of the intergalactic medium (IGM) and also to the underlying cosmological model. Hence it has been extensively used to constrain dark matter [5–14], cosmological [15–21] and astrophysical parameters [22–25]. With large surveys such as ongoing DESI [26–30] and upcoming WEAVE [31, 32], it will become possible to access a large number of QSO spectra, making it important to construct theoretical models and simulations which can be used for interpreting the data. In particular, efficient exploration of the unknown parameter space would require computationally efficient models of the IGM.

One approach for constructing such models is to make some approximation for the baryonic density field and use physical parameters to compute the $\text{Ly}\alpha$ optical depth, for examples of such models see [33, henceforth, A23] and references therein. More recently, there have been approaches based on effective field theory [34], like those used in the study of large-scale structures. A different approach to efficient parameter space exploration is based on machine learning techniques, e.g., using generative neural networks in combination with low-resolution simulations to produce outputs equivalent to high-resolution hydrodynamical simulations [35]. All of these approaches enable, in principle, a joint exploration of the cosmological and astrophysical parameter space. This is particularly important when considering parameters related to dark matter phenomenology (such as, e.g., the mass of a ‘warm’ dark matter candidate) which lead to suppression of power at small scales, since such effects may also arise due to variations in the thermal history of the IGM.

In our earlier work A23, we developed an end-to-end MCMC analysis method to constrain the astrophysical and cosmological parameters using the lognormal approximation.

The lognormal model offers a quick and simplistic way of modelling the IGM. We tested the model in recovering the thermal and ionization parameters against Sherwood simulation, a smooth particle hydrodynamical (SPH) simulation, at $z \sim 2.5$. Building on A23, in this paper we extend the work to other redshifts. We also improve the methodology used in previous work in several ways: (i) We find that the lognormal model, in the usual implementation, is unable to match simultaneously the 1-point probability density function (PDF) and the power spectrum of the SPH simulations. To address this, we take a first step to modify the lognormal model and introduce an additional parameter, ν , to scale the 1D baryonic density field. (ii) Even with this additional parameter, we find that the lognormal model cannot match the flux probability distribution function (FPDF) particularly at high redshifts. We henceforth exclude FPDF from likelihood analysis and only use flux power spectrum (FPS) and mean transmitted flux (\bar{F}). This is a relatively common practice in the literature [36–41], and we leave a more detailed study of the behaviour of the FPDF to future work. (iii) We use a larger path length in SPH sightlines ($DX \sim 16$ compared to ~ 6 previously). This brings the SPH data closer to current high resolution observed data. (iv) We also reduce uncertainty due to our lognormal model by taking a path length twice the size of SPH data (these two path lengths were equal in previous work). (v) We calculate the Ly α optical depth using the density, velocity, and temperature fields provided by SPH instead using optical depth values directly. This ensures identical Γ_{12} values and fitting function for recombination coefficient in both SPH and lognormal.

The layout of the paper is as follows, in §2, we describe in detail the differences (as compared to A23) in methodology for calculating flux statistics, covariance matrices, performing likelihood analysis as well as the introduction of additional parameter. In §3, we present our results of recovering thermal and ionization histories. In §4, we discuss the limitations of lognormal model as well as potential application, and we conclude in §5.

2 Simulations & Method

In this section, we briefly describe the semi-numerical simulations of the Ly α forest based on the lognormal model, the Sherwood SPH simulations used for comparison and the procedure for parameter recovery using likelihood analysis and request the readers to refer to A23 for more details. Throughout this work, we fix cosmological parameters for lognormal to Planck 2014 cosmology, the same being used in Sherwood simulations, $\{\Omega_m = 0.308, \Omega_\Lambda = 1 - \Omega_m, \Omega_b = 0.0482, h = 0.678, \sigma_8 = 0.829, n_s = 0.961, Y = 0.24\}$, consistent with the constraints from [42].

2.1 Lognormal approximation

In our framework, the linearly extrapolated power spectrum of DM density field, $P_{\text{DM}}(k)$, is calculated for given set of cosmological parameters.¹ The 3D power spectrum of the baryonic density fluctuations at any given redshift z is then given by²

$$P_b^{(3)}(k, z) = D^2(z)P_{\text{DM}}(k) e^{-2x_J^2(z)k^2}. \quad (2.1)$$

¹We use the CAMB transfer function [43, <https://camb.readthedocs.io/en/latest/>] to calculate linear matter power spectrum, same as Sherwood simulations [44].

²Unlike in some literature [45, 46], where smoothing is done on the Ly α transmitted flux, we use a more physical way by smoothing the DM density field itself.

where $D(z)$ is the linear growth factor and $x_J(z)$ is the Jeans length. The above relation is based on the assumption that the baryonic fluctuations follow the dark matter at large scales $k^{-1} \gg x_J$ and are smoothed because of pressure forces at scales $k^{-1} \lesssim x_J$. Since the Ly α forest probes the cosmic fields only along the lines of sight, it is sufficient to generate the line of sight baryonic density field $\delta_b^L(x, z)$ and the corresponding line of sight component of the velocity fields $v_b^L(x, z)$ only along one direction. We can obtain the 1D baryonic ($P_b^{(1)}(k, z)$) and linear velocity ($P_v^{(1)}(k, z)$) power spectra from 3D baryonic power spectra by

$$P_b^{(1)}(k, z) = \frac{1}{2\pi} \int_{|k|}^{\infty} dk' k' P_b^{(3)}(k, z), \quad (2.2)$$

and

$$P_v^{(1)}(k, z) = \dot{a}^2(z) k^2 \frac{1}{2\pi} \int_{|k|}^{\infty} \frac{dk'}{k'^3} P_b^{(3)}(k, z), \quad (2.3)$$

where a is the scale factor \dot{a} is given by the Friedman equation

$$\dot{a}^2(z) = H_0^2 \left[\Omega_m(1+z) + \Omega_k + \frac{\Omega_\Lambda}{(1+z)^2} \right], \quad (2.4)$$

with $\Omega_k = 1 - \Omega_m - \Omega_\Lambda$. We then follow procedure given by [47, 48] to generate density and velocity fields along line of sight using eqs. 2.2 and 2.3.

To account for the quasi-linear description of the density field, we employ the lognormal assumption and take the baryonic number density to be

$$n_b(x, z) = A e^{\delta_b^L(x, z)}, \quad (2.5)$$

where A is a normalization constant fixed by setting the average value of $n_b(x, z)$ to the mean baryonic density $\bar{n}_b(z)$ at that redshift.

Given the density and velocity fields of baryons, one can compute the neutral hydrogen field assuming the gas to be in photoionization equilibrium,

$$\alpha_A[T(x, z)] n_p(x, z) n_e(x, z) = n_{\text{HI}}(x, z) \Gamma_{12}(z)/(10^{12} \text{ s}), \quad (2.6)$$

where $\alpha_A(T)$ is the recombination coefficient at temperature T (taken to be of A-type in this work, appropriate for the low-density IGM), n_p, n_e are the number densities of protons and free electrons respectively and Γ_{12} is the hydrogen photoionization rate (in units of 10^{-12} s^{-1} and assumed to be homogeneous). Assuming a fully ionized IGM, n_p, n_e are given by,

$$n_p(x, z) = \frac{4(1-Y)}{4-3Y} n_b(x, z); \quad n_e = \frac{4-2Y}{4-3Y} n_b(x, z) \quad (2.7)$$

where Y (~ 0.24) is helium weight fraction. This requires specifying the IGM temperature at every point, which we do using a power-law temperature-density relation characterized by the temperature T_0 at the mean density and the slope γ , appropriate for the low-density IGM $T(x, z) = T_0(z)[1 + \delta_b^L(x, z)]^{\gamma(z)-1}$. We also need to assume the value of the photoionization rate. The Ly α optical depth is computed by accounting for thermal and natural broadening at each of these grid points x_i ,

$$\begin{aligned} \tau(x_i, z) &= \frac{cI_\alpha}{\sqrt{\pi}} \sum_j \delta x \frac{n_{\text{HI}}(x_j, z)}{b(x_j, z)[1+z(x_j)]} \\ &\times V_\alpha \left(\frac{c[z(x_j) - z(x_i)]}{b(x_j, z)[1+z(x_i)]} + \frac{v_b^L(x_j, z)}{b(x_j, z)} \right), \end{aligned} \quad (2.8)$$

where δx is the separation between the grid points (i.e., the grid size), $I_\alpha = 4.45 \times 10^{-18} \text{ cm}^2$ is the Ly α absorption cross section and $V_\alpha(\Delta v/b)$ is the Voigt profile for the Ly α transition and

$$b(x, z) = \sqrt{\frac{2k_{\text{boltz}}T(x, z)}{m_{\text{p}}}}, \quad (2.9)$$

where m_{p} is the proton mass. It then leads to the main observable, i.e., the normalized Ly α transmitted flux, $F(x_i, z) = e^{-\tau(x_i, z)}$. To mimic observational data, we also convolve $F(x_i, z)$ with Gaussian line spread function of full width at half maximum 7 km s^{-1} as well as add random noise of SNR 50 per pixel. Our model at this stage is thus described by four free parameters, namely, $\{x_{\text{J}}, T_0, \gamma, \Gamma_{12}\}$.

Additionally, we introduce a new free parameter, ν , which scales 1D baryonic density field according to

$$\delta_{\text{b}}^L(x, z) \rightarrow \nu \delta_{\text{b}}^L(x, z). \quad (2.10)$$

We emphasize that we perform this scaling *before* exponentiating δ_{b}^L in equation (2.5). The inclusion of the parameter ν is an attempt to allow the model some freedom in setting the variance of baryonic density fluctuations (which are still distributed as a lognormal). As we already stated in A23, the default model, which corresponds to the case $\nu = 1$, is not a good description of baryonic properties. *Our final model thus contains five free parameters: $\{x_{\text{J}}, T_0, \gamma, \Gamma_{12}, \nu\}$.*

2.2 SPH simulation

To test the validity of our model, we use publicly available Sherwood simulations suite [44] that were performed with a modified version of the cosmological smoothed particle hydrodynamics code P-Gadget-3, an extended version of publicly available GADGET-2 code [49]³. The Sherwood suite consists of cosmological simulation boxes with volume ranging from 10^3 to $160^3 h^{-3} \text{ cMpc}^3$ and contains number particles ranging from 2×512^3 to 2×2048^3 . The size and resolution of simulation box are suitable for studying the small scale structures probed by Ly α forest. The properties of Ly α forest from Sherwood simulation suite are well converged [44]. Similar to A23, as the default, we choose a box of volume $40^3 h^{-3} \text{ cMpc}^3$ containing 2×2048^3 particles.

2.3 Skewer configuration and covariance matrices

The calculation of all relevant statistics including the mean flux, FPS and their covariances for both SPH and lognormal remains similar to A23 (see their equations 12-16). We calculate our "data points" by averaging statistics over 100 skewers picked randomly from a total 5000 available. The SPH covariance matrix is calculated using Jackknife resampling using the entire 50 (=5000/100) realizations. For lognormal covariance matrix, we generate 40000 skewers of same size of that of SPH. To reduce uncertainty from lognormal relative to SPH, the covariance matrix for lognormal is calculated by averaging statistics over 200 skewers. The covariance matrix is then calculated using 200 (=40000/200) realizations without Jackknife resampling. There are other key differences, which we list here:

- In A23, we had used a default path length of $DX \sim 6.2$ (equivalent to averaging over 40 skewers) at $z = 2.5$ in both lognormal and SPH. Additionally, we also considered a *variation* where we averaged SPH and lognormal over 100 and 200 skewers respectively.

³<https://wwwmpa.mpa-garching.mpg.de/gadget/>

Our reasoning was to bring the SPH dataset closer to current observational data and reduce uncertainties arising from lognormal relative to SPH. We consider this *variation* as our *default* configuration throughout this work. Please note that we have average SPH and lognormal over 100 and 200 skewers respectively at all redshifts and vary DX accordingly.

- We exclude FPDF from the likelihood analysis as it gives poor fits at higher redshifts and only use $\{\bar{F} + \text{FPS}\}$ for the said purpose. In \bar{F} , we artificially scale the errors to 5% of mean flux at every redshift in SPH data. The reason to scale the error on \bar{F} is two-fold, (i) results from 2D χ^2 analysis on $\log x_J - \nu$ grid using unscaled error on \bar{F} ($\sim 1\%$ of mean flux) and keeping other parameters fixed to their true values (similar to the results in Figs. 1 and 2) showed minimum $\chi^2_\nu \gtrsim 10$ at all redshifts, implying that the model is unable to recover the true parameters. We were able to ascertain that the poor fits resulted from the inability of lognormal to match \bar{F} within such small error. (ii) The observed mean flux typically has $\sim 5\%$ error arising due to systematic uncertainty in continuum placement [25].

We have run eight Markov Chain Monte Carlo (MCMC) chains using publicly available code `cobaya`⁴[50–52], at $z = \{2, 2.1, 2.2, 2.3, 2.4, 2.5, 2.6, 2.7\}$. To determine when a chain is converged, we use Gelman-Rubin statistics parameter, $R-1 < 0.05$ [51, 53]. The convergence for each chain takes ~ 10 days, using 32 cpus on a 2048 grid with a path length of ~ 16 at $z = 2.5$. All MCMC calculations were performed on the Pegasus cluster at IUCAA.⁵

3 Results

In this section, we present the recovery of the free parameters of the lognormal by comparing with the SPH simulations.

3.1 2-parameter fit

Before presenting MCMC results for our full 5-parameter model described in the previous sections, let us first try to understand what would be the typical value of the Jeans length x_J and ν , parameters which do not have an obvious counterpart in the SPH simulations. Keeping this in mind, we do a simple χ^2 -minimization using a 2D grid in $\log x_J - \nu$ and find the values of $\{x_J, \nu\}$ which best fit the simulation output. For the other three parameters, namely, Γ_{12}, T_0, γ , we use the values as in the SPH simulation. As mentioned earlier, we use the two flux statistics \bar{F} and FPS for calculating the χ^2 . We repeat this exercise at all 8 redshifts.

Fig. 1 shows the colormap plot of χ^2 as a function of x_J and ν for all 8 redshifts. Fig. 2 shows the corresponding best-fit lognormal flux statistics compared with the input SPH. Fig. 4 summarises the redshift evolution of best-fit x_J and ν . At every redshift, we see clear minima in Fig. 1 which provides monotonically decreasing (*w.r.t.* redshift) best-fit values of x_J from $0.23 h^{-1}\text{Mpc}$ at $z = 2$ to $0.11 h^{-1}\text{Mpc}$ at $z = 2.7$ in Fig. 4. This value is of the same order as the one obtained by assuming Ly α absorbers to be in hydrostatic equilibrium at a temperature $\sim 10^4\text{K}$ [54]. The best-fit values of ν do not show such simple monotonic trend, although still decrease as we go from lowest to highest redshift. The minimum reduced χ^2 ,

⁴https://cobaya.readthedocs.io/en/latest/sampler_mcmc.html

⁵<http://hpc.iucaa.in/>

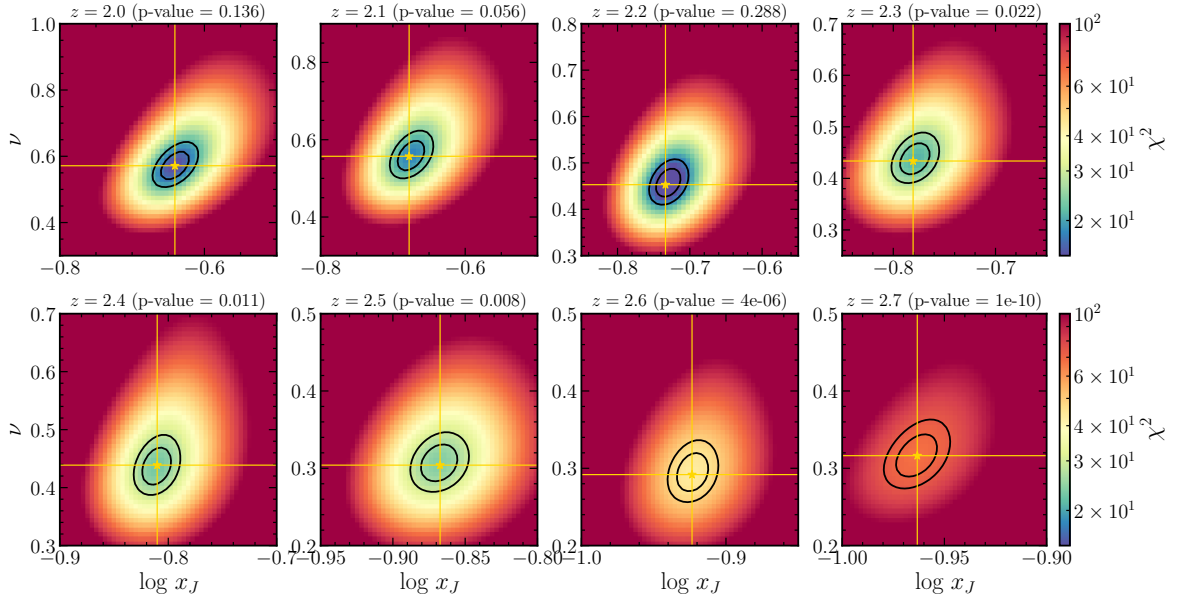


Figure 1. χ^2 colmap on $\log x_J - \nu$ grid with $\{T_0, \gamma, \Gamma_{12}\}$ fixed to their true values for all 8 redshift bins. We get acceptable fits for $z \leq 2.5$. Black contours show 1 and 2- σ confidence levels and gold stars show position of best-fit $\{x_J, \nu\}$. p-values or probability-to-exceed (PTE) are mentioned along side redshift at top of each panel.

$\chi_{\nu, \min}^2$ and p-values for $2 \leq z \leq 2.5$ are $\{1.5, 1.8, 1.2, 2.1, 2.3, 2.4\}$ and $\{0.136, 0.056, 0.288, 0.022, 0.011, 0.008\}$ respectively, which implies that the fit is just acceptable. The fits for $z = 2.6$ and 2.7 are however, quite poor with $\chi_{\nu, \min}^2$ and p-values being $\{4.3, 6.8\}$ and $\{4 \times 10^{-6}, 1 \times 10^{-10}\}$ respectively (Fig. 2). This poor fit implies that the lognormal cannot recover the SPH statistics when the three parameters T_0, γ, Γ_{12} are fixed to the SPH values.

To understand the possible reasons for this failure at higher redshifts, in Fig. 3 we show the 1-point PDF (*left panel*) and power spectrum (*right panel*) of the baryonic number density fluctuation $\Delta_b = n_b/\bar{n}_b$ calculated in the lognormal approximation at three redshifts, using the SPH values for $\{T_0, \gamma, \Gamma_{12}\}$ and the best fit values of $\{x_J, \nu\}$ from the 2-d analysis described above. To our knowledge this is the first comparison of Δ_b statistics between SPH and a lognormal model weakly adjusted to fit the \bar{F} and FPS statistics. It is quite apparent that neither the PDF nor the power spectrum of Δ_b the lognormal model agree well with the SPH quantities at any redshift. Nevertheless, at least at low redshifts $z \simeq 2.0$, the model produces a completely acceptable fit to the FPS and \bar{F} measurements. E.g., it is striking that the orders of magnitude difference between the power spectra at $z = 2$ (red solid and dashed curves in the *right panel* of Fig. 3) is consistent with the excellent match in FPS and \bar{F} seen in the blue curves in Fig. 2. Simultaneously, the mean of $\log \Delta_b$ is clearly higher in this best fitting lognormal model than in the SPH. The power spectrum conundrum might be partially attributed to the fact that the FPS is a highly smoothed version (due to the Voigt kernel) of a highly nonlinear transform of Δ_b , such that the scales relevant for calculating the FPS from Δ_b are restricted to small k (indeed, the conventional wisdom is that these are ‘quasi-linear’ scales). The mismatch in PDF of Δ_b , however, leaves a distinct imprint in the comparison of \bar{F} values: \bar{F} is systematically smaller in the best fitting lognormal model than in the SPH, with the difference becoming more pronounced

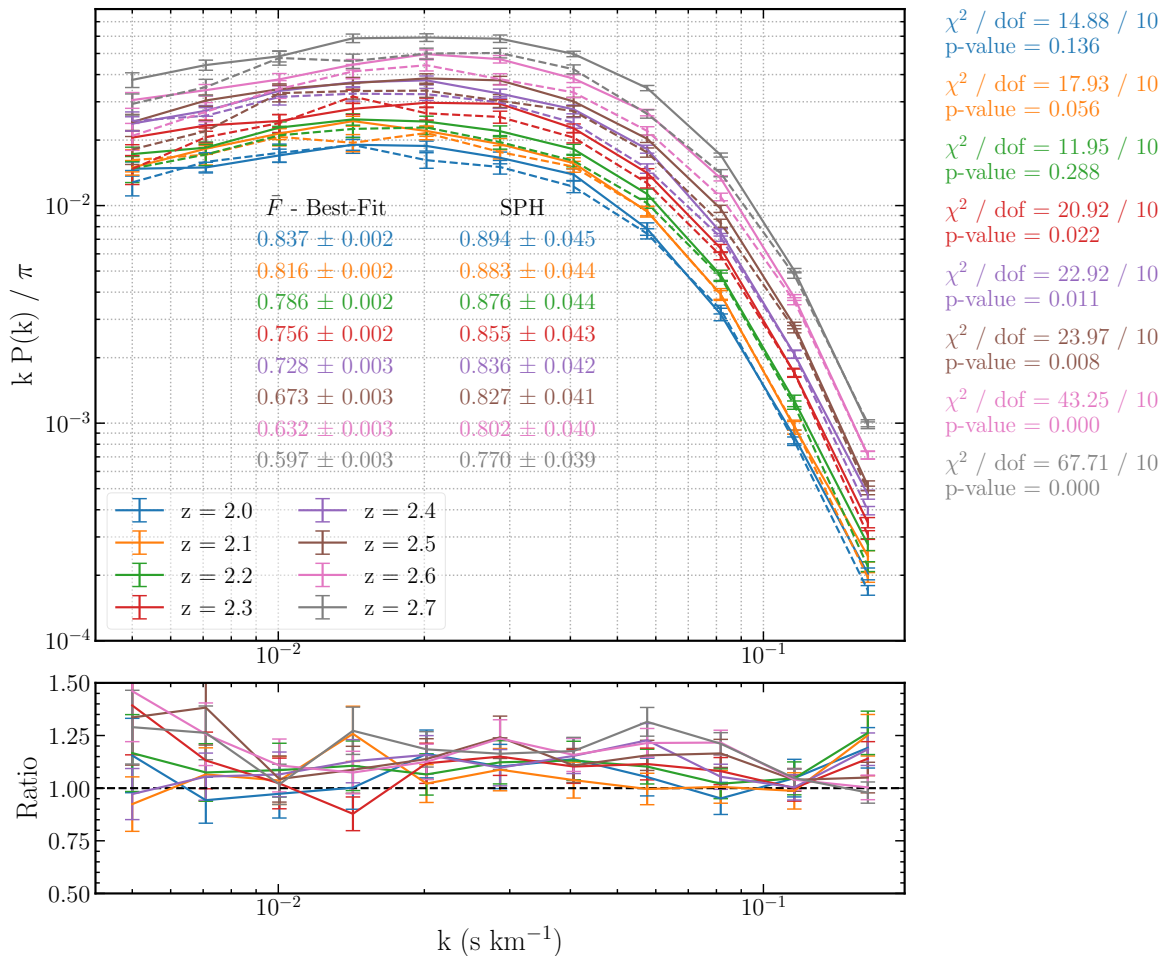


Figure 2. Flux statistics for SPH data and best-fit parameters obtained from 2D χ^2 analysis. Solid curves are best-fit lognormal and dashed curves are SPH.

(and more statistically significant) at larger redshifts (where the quality of the overall fit also degrades). This can be qualitatively understood in the context of the mismatch in the PDF of Δ_b ; the overestimate of volume occupied by mildly overdense regions $\Delta_b \sim 1-3$ in the lognormal directly implies an underestimate of overall flux $F = e^{-\tau}$ at fixed photoionization rate, assuming that τ is approximately monotonic with Δ_b and that only mildly overdense regions contribute to Ly α flux.

These arguments are not complete by any means, however. The $z = 2$ results especially indicate that a substantial role might be played by higher order statistics (non-Gaussianities) of the baryonic log-density field, which the lognormal model simply sets to zero. The impact of these non-Gaussianities on the FPS and \bar{F} has not been explored in the literature, to our knowledge. We leave such a study to future work. For now, we simply note that, despite the degrees of freedom provided by x_J and ν , the lognormal model constrained by Ly α flux statistics is unable to match the 1-point and 2-point statistics of the baryonic density fields. This suggests that, when varying all 5 model parameters, *at least* one of the parameters $\{T_0, \gamma, \Gamma_{12}\}$ is likely not to be recovered with good accuracy. The arguments above would indicate that this parameter is likely to be the photoionization rate Γ_{12} , due to its impact on

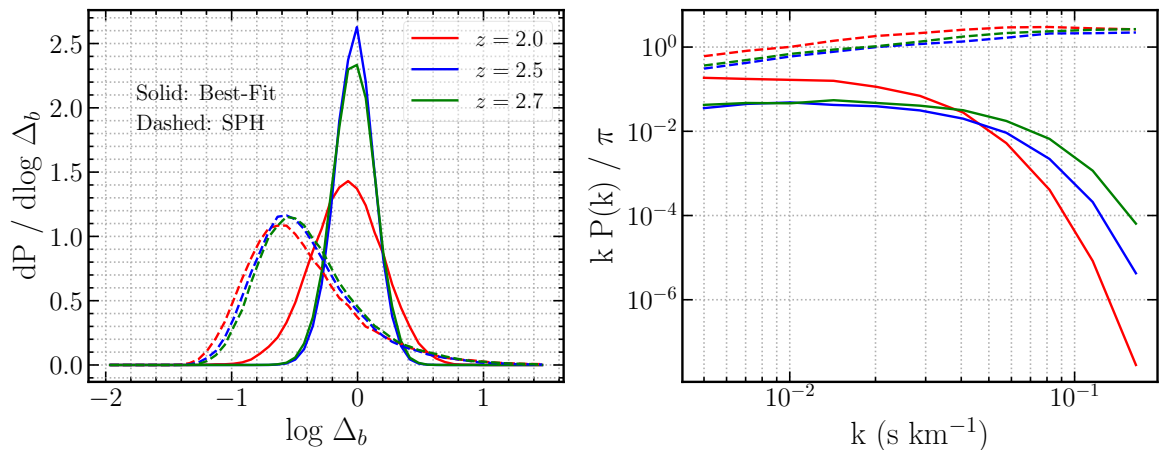


Figure 3. 1-point PDF of $\log \Delta_b$ (left) and power spectrum of Δ_b (right) for best-fit $\{x_J-\nu\}$, keeping $\{T_0, \gamma, \Gamma_{12}\}$ fixed to their true values (solid curves), along with statistics for SPH (dashed curves).

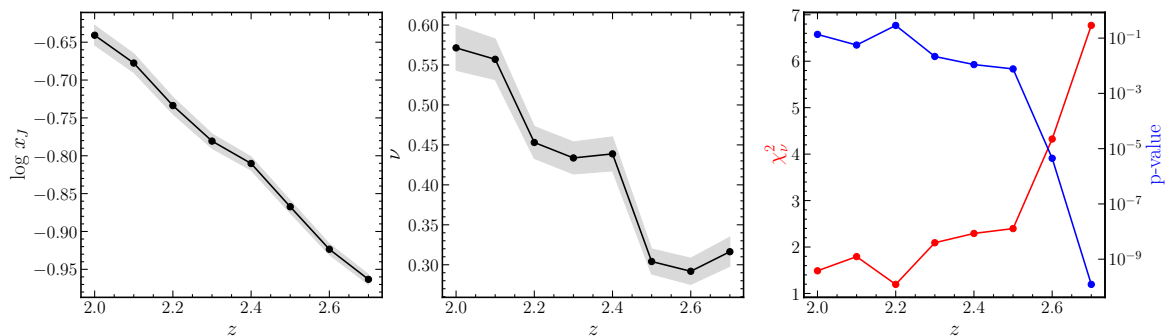


Figure 4. First and second panels show redshift evolution of best-fit x_J and ν from 2D χ^2 analysis and true values of $\{T_0, \gamma, \Gamma_{12}\}$ (black curves). Third panel shows minimum χ^2_ν (red) and corresponding p-value (blue) at each redshift.

\bar{F} .

Keeping this in mind, we proceed as in A23 to vary all the model parameters simultaneously in the next section. We will return to a discussion of the quality of parameter recovery in section 4.

3.2 5-parameter fit

In this section, we explore the case where all the free parameters of the lognormal are allowed to vary. Table 1 lists the priors on parameters, $\{\log x_J, \log T_0, \gamma, \log \Gamma_{12}, \nu\}$. While we have used simple, flat, and wide priors on four parameters, $\{\log T_0, \gamma, \log \Gamma_{12}, \nu\}$, we have imposed a more physically motivated prior on $\log x_J$ by calculating the lower limit on the prior, $x_{J,\text{th}}$, using equation

$$x_{J,\text{th}} = \frac{1}{H_0} \left[\frac{2\gamma_s k_B T_{0,s}}{3\mu m_p \Omega_m (1+z)} \right]^{1/2} \quad (3.1)$$

where $T_{0,s}$ and γ_s are values of T_0 and γ sampled in the MCMC chain respectively. For reference, the values of $\log x_{J,\text{th}}$ at redshifts $\{2.0, 2.1, 2.2, 2.3, 2.4, 2.5, 2.6, 2.7\}$ for corresponding

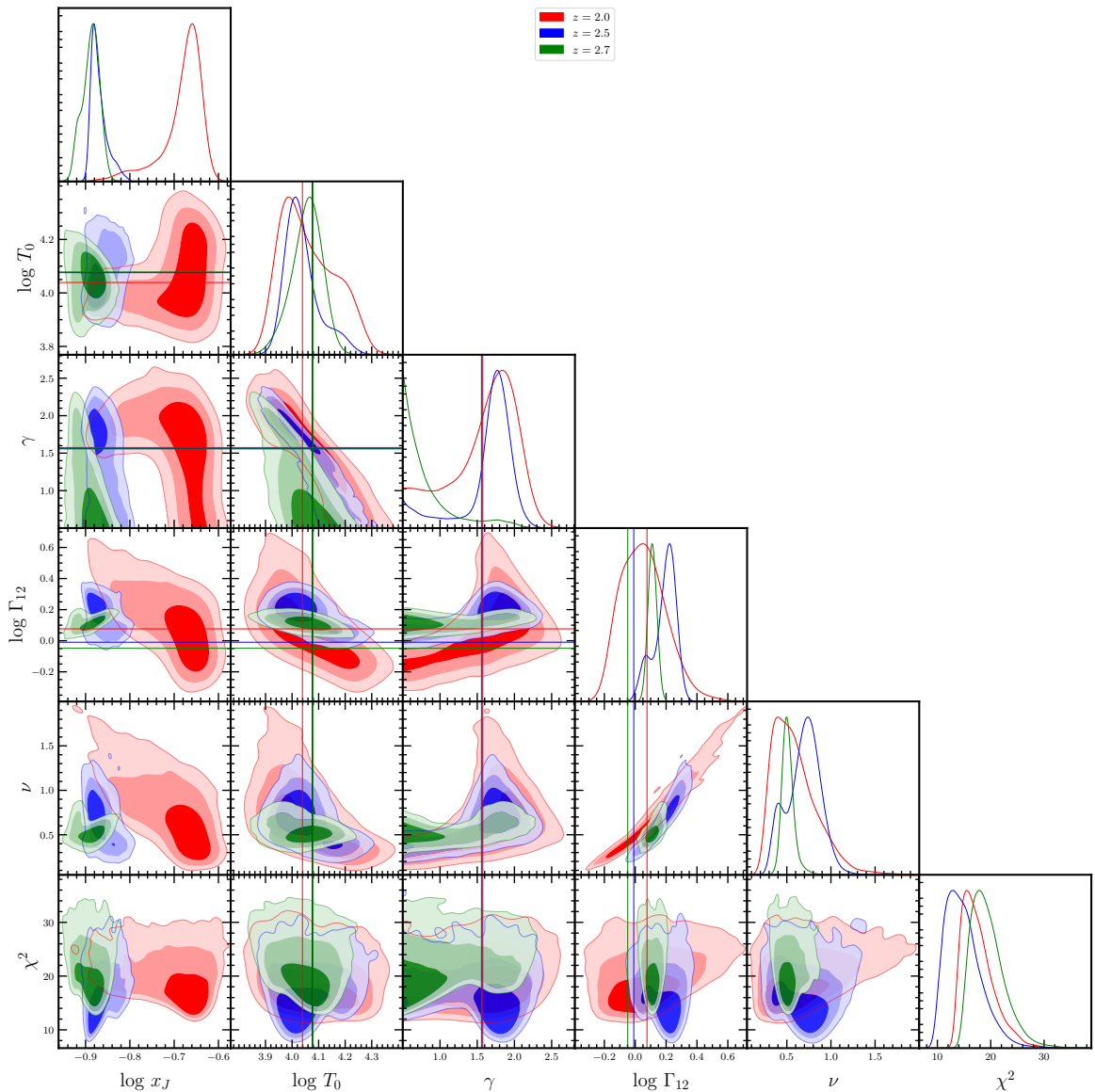


Figure 5. 1, 2, and 3- σ contours for three redshifts, $z = 2, 2.5,$ and 2.7 . Colour coded horizontal and vertical lines show true values of parameters.

true values of T_0 and γ are $\{-0.877, -0.879, -0.879, -0.883, -0.895, -0.900, -0.905\}$ respectively. The motivation behind imposing the limit from eq.3.1 is that lognormal model tends to favor unphysically small values of x_J , $\sim 0.01 h^{-1}\text{Mpc}$ at high redshifts. The upper limit on the prior (for $\log x_J$) is fixed to 0.5.

The true values (i.e., the values used in or obtained from the SPH simulations) along with best-fit and median of the parameters at each redshift are reported in Table 2. In figs. 5, 6, and 7 we show the contour plots (68.3, 95.4, 99.7 percentiles) for three redshifts, $z = 2, 2.5,$ and 2.7 , obtained from MCMC run, corresponding best-fit and SPH flux statistics, and the evolution of best-fit values of parameters with redshift respectively. From Fig. 7, it is evident that the lognormal model does a decent job at recovering T_0 at all redshifts with

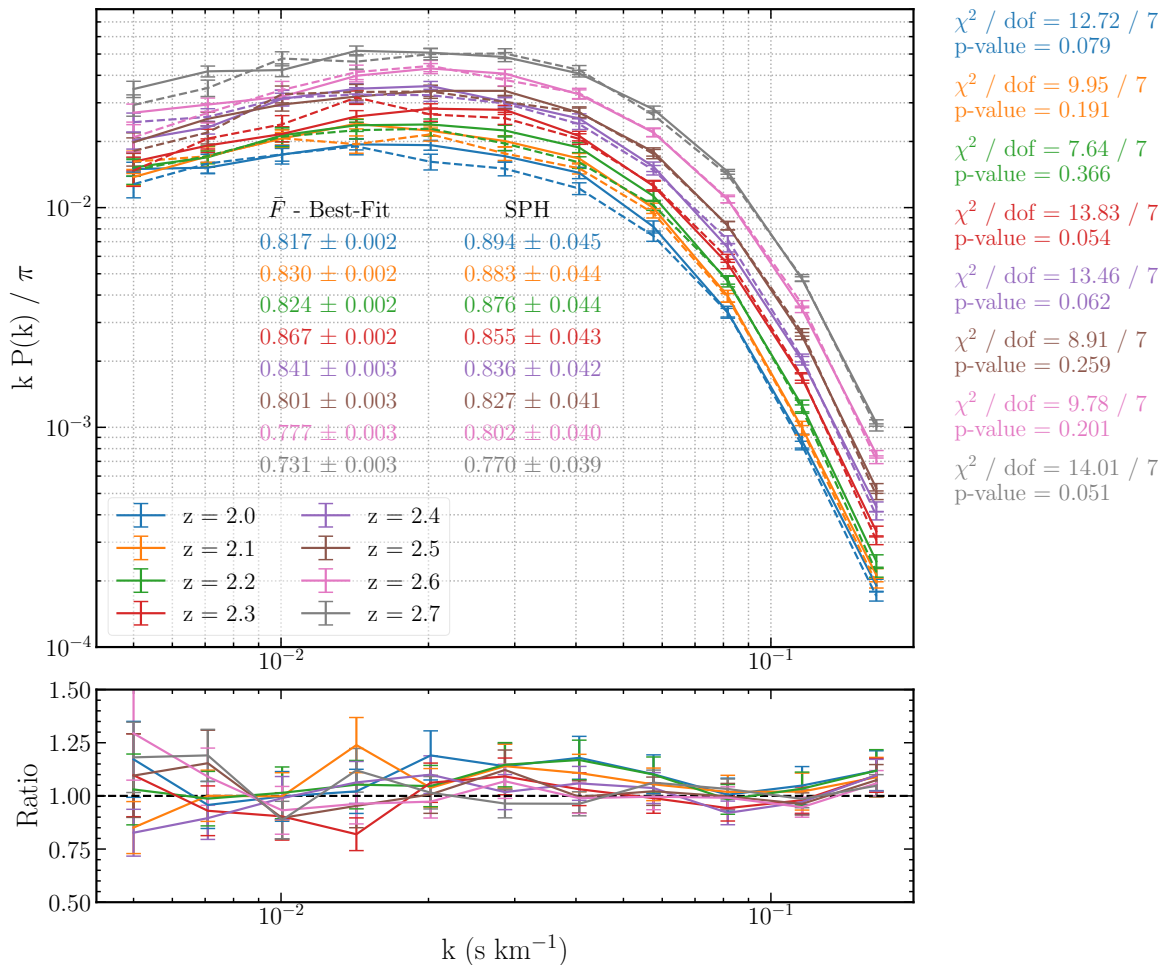


Figure 6. Flux statistics for best-fit model and SPH data for all the redshifts.

Parameter	Prior
$\log x_J$	$[\log x_{J,\text{th}}, 0.5]$
$\log T_0$	$[2.5, 5.5]$
γ	$[0.5, 5]$
$\log \Gamma_{12}$	$[-2, 2]$
ν	$[0.05, 2]$

Table 1. Priors on parameters, $\{\log x_J, \log T_0, \gamma, \log \Gamma_{12}, \nu\}$, where $\log x_{J,\text{th}}$ is calculated using eq.3.1. See text for a discussion of the parameter x_J .

the true values being within $1-\sigma$ from the median. γ , although, is recovered reasonably well at all redshifts except $z = 2.7$, has a tendency to favor bimodality with an "inverted" $T - \Delta_b$ relation. At $z = 2.7$, γ has completely hit the prior. Another limitation of lognormal model is in estimating Γ_{12} . In fig.7, we can see (i) Γ_{12} is recovered within $1-\sigma$ only till $z = 2.2$ and (ii) shape of evolution of Γ_{12} *w.r.t* redshift from lognormal is in complete disagreement with that of SPH. From both figs. 5 and 7, we also observe degeneracies between $T_0 - \gamma$ and $\Gamma_{12} - \nu$. These degeneracies may significantly affect parameter estimates. E.g., underestimating value

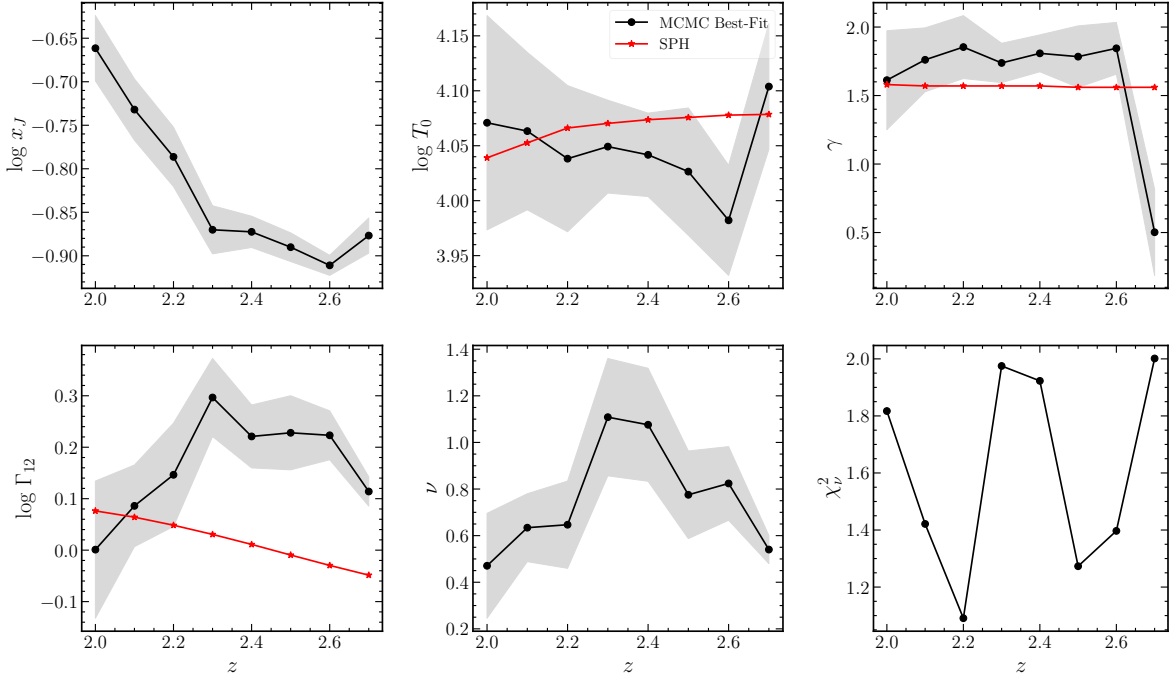


Figure 7. Redshift evolution of parameters and reduced χ^2 shown with black circles. Gray shaded regions 16 and 84 percentiles from MCMC chains. Red triangles are true values of parameters in SPH.

of γ at $z = 2.7$ has overestimated T_0 . Although in this particular case the strong anti-correlation has made the estimate of T_0 better. On the other hand, we see a strong positive correlation in Γ_{12} and ν where shapes of redshift evolution curves of both parameters are remarkably similar.

Thus, as anticipated earlier, the lognormal model cannot simultaneously recover the true values of all the parameters $\{T_0, \gamma, \Gamma_{12}\}$ and it is indeed Γ_{12} that is affected the most. We discuss this aspect of the model in more detail in the next section.

4 Discussion

In this section we present a qualitative argument to understand the failure of the lognormal model seen above, followed by a discussion of potential cosmological applications of the model as it stands.

4.1 Recovery of Γ_{12}

The fact that the failure of the lognormal model in parameter recovery mostly manifests in the poor recovery of Γ_{12} can be understood as follows. Γ_{12} appears in the model entirely as a multiplicative factor in calculating the neutral hydrogen number density $n_{\text{HI}} \propto \Gamma_{12}^{-1}$. This subsequently propagates to the optical depth $\tau(z) \sim \int dz' n_{\text{HI}}(z') K(z, z')$, where the nature of the kernel K is irrelevant for this argument since it does not involve Γ_{12} (so we can also simply approximate $\tau \sim n_{\text{HI}}$ as far as Γ_{12} and ν are concerned). Thus $\tau \propto \Gamma_{12}^{-1}$ due to the dependence on n_{HI} . However, since $n_{\text{HI}} \propto n_b^\beta$ where β is order unity, the *fluctuations* in τ (at least at large scales) scale proportionally to the parameter ν . Thus, fluctuations in τ have

the overall approximate dependence $\delta\tau \propto \nu \Gamma_{12}^{-1}$, making ν and Γ_{12} highly degenerate when determining the power spectrum of the flux $F = e^{-\tau}$, and explaining the strong positive degeneracy mentioned above.

We further note that using the true value of Γ_{12} leads to rather small values of ν in the previous 2-d analysis (Fig. 1). Simultaneously, the best fitting model leaves behind a mean flux $\bar{F} = \langle e^{-\tau} \rangle$ that is significantly smaller than the SPH, and an FPS that is significantly larger, especially at higher redshifts (see Fig. 2). This is consistent with our earlier discussion regarding the fact that the lognormal approximation does not simultaneously describe the 1-point and 2-point functions of the baryonic density field.

Once Γ_{12} is also allowed to vary, the model can accommodate a larger value of \bar{F} and smaller FPS by increasing both ν and Γ_{12} . To understand why, it is again useful to approximate $\Delta_b \simeq 1 + \delta_b^L$, so that $\tau \sim n_{\text{HI}} \sim n_b^\beta / \Gamma_{12} \sim \bar{n}_b^\beta (1 + \beta \delta_b^L) / \Gamma_{12}$. The key point to note here is that Γ_{12} multiplies both the mean and fluctuations of τ , while ν appears only in the fluctuations, through δ_b^L . We can then approximate

$$\tau = \bar{\tau} + \delta\tau \sim C_1 / \Gamma_{12} + C_2 (\nu / \Gamma_{12}) \hat{g}, \quad (4.1)$$

where C_1 and C_2 don't depend on ν or Γ_{12} and \hat{g} is a Gaussian distributed random variable with zero mean and unit variance. As compared to C_1 , the quantity C_2 involves the amplitude of density fluctuations, so we expect $C_2 \ll C_1$. This gives us

$$\begin{aligned} F &= e^{-\tau} \sim e^{-C_1 / \Gamma_{12} - C_2 (\nu / \Gamma_{12}) \hat{g}}, \\ \bar{F} &\simeq e^{-\bar{\tau} + \langle \delta\tau^2 \rangle / 2} \sim e^{-C_1 / \Gamma_{12} + C_2^2 (\nu / \Gamma_{12})^2 / 2} \sim e^{-C_1 / \Gamma_{12}}, \\ \delta_F &\equiv F / \bar{F} - 1 \simeq e^{-\delta\tau - \langle \delta\tau^2 \rangle / 2} - 1 \simeq -\delta\tau, \\ P_F &\sim \langle \delta_F^2 \rangle \sim \langle \delta\tau^2 \rangle \sim C_2^2 (\nu / \Gamma_{12})^2. \end{aligned} \quad (4.2)$$

We now consider the fact that, with $\nu = 1$ and $\Gamma_{12} = \Gamma_{12}^{(\text{SPH})}$, the lognormal model produces a FPS (\bar{F}) that substantially overestimates (underestimates) that from SPH. If Γ_{12} is fixed, the only available degree of freedom is ν , which is driven to small values that decrease the FPS (since $P_F \propto \nu^2$) and *also decrease* \bar{F} (since $\bar{F} \sim e^{\# \nu^2}$ when only ν is varied). Note that arbitrarily small values of $\nu \rightarrow 0$ are strongly disfavoured by the FPS, which would be driven to zero in this case. The variation of Γ_{12} in the full analysis now becomes significant; increasing Γ_{12} *increases* the value of \bar{F} in the the lognormal model, since $\bar{F} \sim e^{-C_1 / \Gamma_{12}}$ (we argued above that the contribution of the term involving C_2 will be subdominant compared to that involving C_1). The interplay between ν and Γ_{12} then balances out to match the FPS. The remaining leeway in achieving this balance shows up as the degeneracy between ν and Γ_{12} we commented on earlier. Consistently with this argument, we have found that *excluding* \bar{F} from the inference leads to an essentially unbroken degeneracy between ν and Γ_{12} , which also highlights the important role played by the \bar{F} constraint in our analysis.

Evidently, the upshot is that a reasonably good fit to the FPS and \bar{F} from SPH can, in fact, be achieved by the lognormal model, at the cost of significantly *overestimating* Γ_{12} (Fig. 7). This might also be understood in a simpler manner, using the comparison of the 1-point PDF of Δ_b between SPH and lognormal in Fig. 3. There, we saw that the lognormal model with any reasonable value of ν significantly over-predicts the number of pixels having $\Delta_b \sim 1-3$, which is where one expects the Ly α forest to arise from. To compensate for this overestimate of potential neutral absorber systems, the model must increase the photoionization rate. As we mentioned earlier, this simple argument also indicates that the eventual

Redshift	$\log x_J$ ($h^{-1}\text{Mpc}$)	$\log T_0$ (K)	γ	$\log \Gamma_{12}$ (10^{-12} s^{-1})	ν
2.0	- / -0.66(-0.67 $^{+0.03}_{-0.05}$)	4.04 / 4.07(4.03 $^{+0.12}_{-0.08}$)	1.58 / 1.61(1.75 $^{+0.28}_{-0.44}$)	0.08 / 0.00(0.07 $^{+0.14}_{-0.13}$)	- / 0.47(0.58 $^{+0.26}_{-0.19}$)
2.1	- / -0.73(-0.74 $^{+0.03}_{-0.04}$)	4.05 / 4.06(4.06 $^{+0.08}_{-0.06}$)	1.57 / 1.76(1.77 $^{+0.23}_{-0.24}$)	0.07 / 0.09(0.10 $^{+0.08}_{-0.08}$)	- / 0.63(0.68 $^{+0.16}_{-0.13}$)
2.2	- / -0.79(-0.79 $^{+0.03}_{-0.04}$)	4.07 / 4.04(4.05 $^{+0.08}_{-0.05}$)	1.57 / 1.85(1.77 $^{+0.21}_{-0.25}$)	0.05 / 0.15(0.15 $^{+0.10}_{-0.10}$)	- / 0.65(0.66 $^{+0.20}_{-0.17}$)
2.3	- / -0.87(-0.84 $^{+0.03}_{-0.02}$)	4.07 / 4.05(4.03 $^{+0.05}_{-0.04}$)	1.57 / 1.74(1.78 $^{+0.16}_{-0.14}$)	0.03 / 0.30(0.25 $^{+0.07}_{-0.08}$)	- / 1.11(0.97 $^{+0.26}_{-0.25}$)
2.4	- / -0.87(-0.86 $^{+0.02}_{-0.01}$)	4.07 / 4.04(4.03 $^{+0.04}_{-0.04}$)	1.56 / 1.81(1.83 $^{+0.14}_{-0.13}$)	0.01 / 0.22(0.19 $^{+0.05}_{-0.07}$)	- / 1.08(0.96 $^{+0.24}_{-0.25}$)
2.5	- / -0.89(-0.87 $^{+0.02}_{-0.01}$)	4.08 / 4.03(4.02 $^{+0.07}_{-0.05}$)	1.56 / 1.78(1.74 $^{+0.18}_{-0.27}$)	-0.01 / 0.23(0.20 $^{+0.06}_{-0.09}$)	- / 0.78(0.70 $^{+0.17}_{-0.21}$)
2.6	- / -0.91(-0.90 $^{+0.01}_{-0.01}$)	4.08 / 3.98(3.99 $^{+0.06}_{-0.05}$)	1.56 / 1.85(1.79 $^{+0.17}_{-0.21}$)	-0.03 / 0.22(0.20 $^{+0.04}_{-0.06}$)	- / 0.82(0.74 $^{+0.14}_{-0.17}$)
2.7	- / -0.88(-0.88 $^{+0.02}_{-0.02}$)	4.08 / 4.10(4.05 $^{+0.05}_{-0.06}$)	1.56 / 0.50(0.77 $^{+0.44}_{-0.19}$)	-0.05 / 0.11(0.11 $^{+0.03}_{-0.03}$)	- / 0.54(0.50 $^{+0.07}_{-0.06}$)

Table 2. True / best-fit(median) values for the parameters explored in MCMC run. Please see that x_J and ν do not have any "true" values.

resolution of the fact that the lognormal model fails to accurately reproduce Ly α flux statistics is likely related to understanding the higher moments of the baryonic log-density field (which the lognormal model treats as Gaussian distributed). Simple fixes such as the inclusion of the scaling parameter ν clearly have their limitations. Addressing this challenge while retaining the simplicity of this semi-analytical model is the subject of work in progress.

4.2 Potential application

It is evident from the preceding discussion that Γ_{12} cannot be reliably estimated using the present form of the lognormal model. Nevertheless, given its success in recovering the remaining IGM parameters, it is interesting to ask whether this model can still be used for *cosmological* parameter inference. This might be the case if, e.g., the cosmological parameter directions are largely independent of Γ_{12} in the space defined by the likelihood function.

Here, we present a preliminary analysis to address this question. In Fig. 8, we show the effect on the lognormal FPS of individually changing the cosmological parameters, $\{\Omega_m, \sigma_8\}$, and the parameter Γ_{12} . We work at $z = 2$ where the lognormal model performs best.⁶ Black curves show FPS for a set of fiducial parameters where the cosmological parameters, $\{\Omega_m, h, \sigma_8, n_s\}$, and the astrophysical parameters, $\{T_0, \gamma, \Gamma_{12}\}$ are fixed to their true values, x_J is the best-fit value from 2D χ^2 analysis and ν is set to unity. In red (blue) curves, we decrease (increase) the parameters by 20% one by one, keeping other parameters fixed. We find that Γ_{12} affects FPS in relatively simplistic way, as in decreasing (increasing) Γ_{12} increases (decreases) power at all scales. This is fully consistent with our qualitative discussion in the previous section. The effects of $\{\Omega_m, \sigma_8\}$, on the other hand, are more complicated. Changing these parameters "tilts" the FPS about some scale k . Given the fact that the nature of this effect is very different from that of Γ_{12} , we can speculate that Γ_{12} would be non-degenerate with the two cosmological parameters. However, we would like to emphasize that Fig. 8 does not show that Γ_{12} and $\{\Omega_m, \sigma_8\}$ are uncorrelated (which would require a full MCMC analysis). Any correlation between them might potentially systematically bias cosmological parameters.

It will be very interesting to study the results of simultaneously varying the astrophysical parameters (which can vary with redshift) and cosmological parameters (which enter the model at each redshift in the same manner) to simultaneously model the SPH data over a broad range of redshifts such as, e.g., $2 \leq z \lesssim 2.5$. We leave this analysis to future work.

⁶Unlike the spectra generated in previous cases, where we use CAMB matter power spectrum, here we use linear power spectrum of [55] to generate the Gaussian density field since we require to vary cosmological

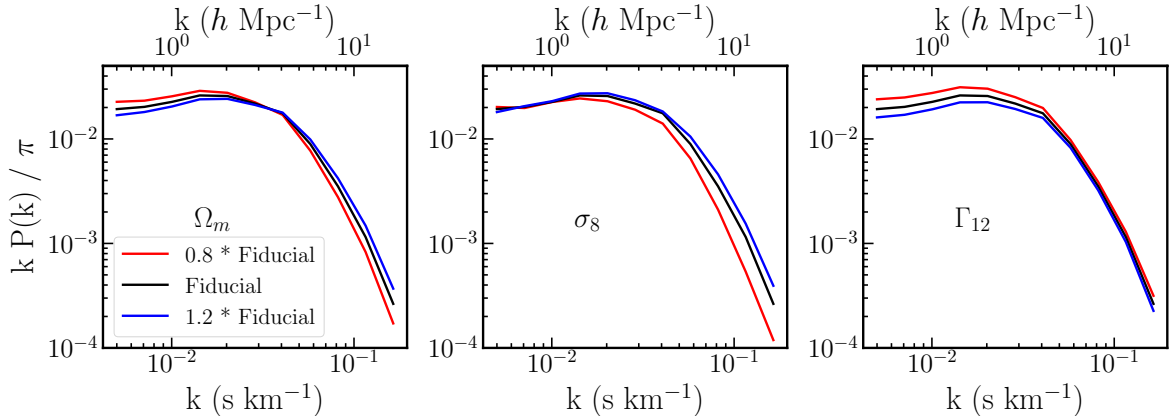


Figure 8. Effect of parameters, $\{\Omega_m, \sigma_8, \Gamma_{12}\}$ on flux power spectrum produced by lognormal model at $z = 2$. Black curves show FPS for a set of fiducial parameters while in red (blue) curves, we decrease (increase) parameters by 20% one by one, keeping other parameters fixed. We observe that changing cosmological parameters, $\{\Omega_m, \sigma_8\}$, tilts the FPS about a pivot scale (although these pivot scales are different), whereas changing Γ_{12} roughly changes the amplitude.

4.3 Comparison with other methods

As stated in A23, various semi-numerical methods have been developed to efficiently simulate Ly α forest, with potential applications in parameter space exploration. The density and velocity distributions in these models are either generated using cosmological N-body simulations or using physically motivated approximations. We have herein, briefly described few such approaches to further emphasize the strengths as well as weaknesses of lognormal model when compared against them. Few such methods include:

- Assuming baryons trace dark matter in simulations [56, 57]. The simplest technique is to assume the baryonic density field perfectly traces the dark matter dark matter field. While this is a safe approximation at large scales, pressure effects cannot be ignored at small scales. Our work accounts for these pressure effects to some extent, by smoothing the dark matter density field using a Gaussian filter.
- Simulating few handful of full hydrodynamic simulations for parameters corresponding to a "best-guess" model and Taylor expanding the observables around those best-guess values [28, 58]. The method considerably reduces the computation cost by eliminating the need for running large number of hydrodynamical simulations but can be inaccurate for large displacements in parameter space and is prone to underestimating errors on recovered parameters due to unaccounted errors in approximation. The immense speed of lognormal model allows us to directly calculate the flux statistics at every point in parameter space, thereby eliminating the uncertainty induced from Taylor expansion.
- Running a large number of inexpensive simulations (e.g., hydro-particle-mesh (HPM)) on a parameter grid and calibrating them using a small number of full hydrodynamic simulations [59, 60]. The method is shown to produce substantially more accurate clustering statistics than Fluctuating Gunn-Peterson Approximation (FGPA) but still remains computationally challenging.

parameters.

- Using emulators based on Gaussian processes / neural network / machine learning to predict flux statistics at any given set of parameters from a small number of full hydrodynamical simulations [41, 61, 62]. E.g., In [41], authors have built emulators capable of reproducing various flux statistics with accuracy upto $\lesssim 2\%$, much better than our work. Despite this, the ease of implementation of the lognormal approximation makes it a viable option.

5 Conclusions

Efficient semi-numerical models of the Ly α forest are expected to play an important role in interpreting the high-quality data obtained from QSO absorption spectra surveys. The focus of this work is to build on our earlier work A23 and understand the effectiveness of one such model, namely, the lognormal model of baryonic densities, in recovering the thermal and ionization properties of the IGM. This is done by comparing the lognormal model with Sherwood SPH simulations [44] across redshifts $2 \leq z \leq 2.7$ and investigate the recovery of the thermal parameters T_0 and γ and the photoionization rate Γ_{12} . We employ an MCMC based method to carry out the comparison, using two transmitted flux statistics: the mean flux and the flux power spectrum $P(k)$.

We find that the conventional lognormal model where the baryonic density is related to the linearly extrapolated density contrast as $n_b \propto e^{\delta_b^L}$ is unable to recover the parameters reliably. This is related to the fact that the model is a poor description of the underlying baryonic density PDF obtained from the Sherwood simulations. We address this limitation by extending the model through a scaling parameter ν such that $n_b \propto e^{\nu \delta_b^L}$. This extension provides a better match to the SPH. In particular, the thermal parameters T_0 and γ are recovered within $1 - \sigma$ of the SPH values. However, the recovery of the photoionization rate Γ_{12} is still discrepant with respect to the SPH, by $\gtrsim 3 - \sigma$ for $z > 2.2$. We explore the reason for this discrepancy in some detail, and conclude that one requires more advanced modelling of the baryonic density PDF in order to overcome this limitation.

This work opens up the possibility of using lognormal approximation to generate mock catalogs and calculate covariance matrices for large volume cosmological surveys such as DESI, WEAVE etc. Furthermore, the ability of lognormal approximation to generate arbitrary long skewers can allow us to study the cross-correlations in flux statistics across different redshift bins, which we have attempted in [63]. Additionally, the fact that lognormal is able to recover thermal history with 20% accuracy can help us set parameters for initial sampling in full hydrodynamical simulations, and / or narrow down the range of priors thus reducing significant computing time. We also speculate that, in spite of the fact that lognormal approximation is unable to recover Γ_{12} , the model can be useful for constraining cosmological parameters. This is demonstrated by showing that the dependencies of the flux statistics, in particular $P(k)$, on the Γ_{12} and the cosmological parameters are quite different. This indicates that one may still be able to use the model for cosmological constraints even when the recovery of Γ_{12} is unreliable. We will explore this possibility in a future project.

Acknowledgments

We thank R. Srianand for useful discussions. We gratefully acknowledge use of the IUCAA High Performance Computing (HPC) facility. We thank the Sherwood simulation team for making their data publicly available. The research of AP is supported by the Associates programme of ICTP, Trieste.

Data Availability

The Sherwood simulations are publicly available at <https://www.nottingham.ac.uk/astronomy/sherwood/index.php>. The data generated during this work will be made available upon reasonable request to the authors.

References

- [1] M. Rauch, *The Lyman alpha forest in the spectra of quasistellar objects*, *Annual Review of Astronomy and Astrophysics* **36** (1998) 267–316, [<https://doi.org/10.1146/annurev.astro.36.1.267>].
- [2] D. H. Weinberg, *The Lyman- α forest as a cosmological tool*, in *AIP Conference Proceedings*, AIP, 2003. DOI.
- [3] A. A. Meiksin, *The physics of the intergalactic medium*, *Reviews of Modern Physics* **81** (oct, 2009) 1405–1469.
- [4] M. McQuinn, *The evolution of the intergalactic medium*, *Annual Review of Astronomy and Astrophysics* **54** (sep, 2016) 313–362.
- [5] S. H. Hansen, J. Lesgourgues, S. Pastor and J. Silk, *Constraining the window on sterile neutrinos as warm dark matter*, *Monthly Notices of the Royal Astronomical Society* **333** (07, 2002) 544–546, [<https://academic.oup.com/mnras/article-pdf/333/3/544/3218304/333-3-544.pdf>].
- [6] M. Viel, J. Lesgourgues, M. G. Haehnelt, S. Matarrese and A. Riotto, *Constraining warm dark matter candidates including sterile neutrinos and light gravitinos with WMAP and the Lyman-alpha forest*, *Physical Review D* **71** (mar, 2005) .
- [7] J. Baur, N. Palanque-Desabrouille, C. Yèche, A. Boyarsky, O. Ruchayskiy, É. Armengaud et al., *Constraints from Ly- α forests on non-thermal dark matter including resonantly-produced sterile neutrinos*, *J. Cosmology Astropart. Phys.* **2017** (Dec., 2017) 013, [[1706.03118](https://arxiv.org/abs/1706.03118)].
- [8] V. Iršič, M. Viel, M. G. Haehnelt, J. S. Bolton, S. Cristiani, G. D. Becker et al., *New constraints on the free-streaming of warm dark matter from intermediate and small scale Lyman- α forest data*, *Phys. Rev. D* **96** (July, 2017) 023522, [[1702.01764](https://arxiv.org/abs/1702.01764)].
- [9] S. Bose, M. Vogelsberger, J. Zavala, C. Pfrommer, F.-Y. Cyr-Racine, S. Bohr et al., *ETHOS - an Effective Theory of Structure Formation: detecting dark matter interactions through the Lyman- α forest*, *MNRAS* **487** (July, 2019) 522–536, [[1811.10630](https://arxiv.org/abs/1811.10630)].
- [10] A. Garzilli, A. Magalich, T. Theuns, C. S. Frenk, C. Weniger, O. Ruchayskiy et al., *The Lyman- α forest as a diagnostic of the nature of the dark matter*, *MNRAS* **489** (Nov., 2019) 3456–3471, [[1809.06585](https://arxiv.org/abs/1809.06585)].
- [11] N. Palanque-Desabrouille, C. Yèche, N. Schöneberg, J. Lesgourgues, M. Walther, S. Chabanier et al., *Hints, neutrino bounds, and WDM constraints from SDSS DR14 Lyman- α and Planck full-survey data*, *J. Cosmology Astropart. Phys.* **2020** (Apr., 2020) 038, [[1911.09073](https://arxiv.org/abs/1911.09073)].
- [12] C. Pedersen, A. Font-Ribera, T. D. Kitching, P. McDonald, S. Bird, A. Slosar et al., *Massive neutrinos and degeneracies in Lyman-alpha forest simulations*, *J. Cosmology Astropart. Phys.* **2020** (Apr., 2020) 025, [[1911.09596](https://arxiv.org/abs/1911.09596)].
- [13] A. Garzilli, A. Magalich, O. Ruchayskiy and A. Boyarsky, *How to constrain warm dark matter with the Lyman- α forest*, *MNRAS* **502** (Apr., 2021) 2356–2363, [[1912.09397](https://arxiv.org/abs/1912.09397)].
- [14] A. K. Sarkar, K. L. Pandey and S. K. Sethi, *Using the redshift evolution of the Lyman- α effective opacity as a probe of dark matter models*, *J. Cosmology Astropart. Phys.* **2021** (Oct., 2021) 077, [[2101.09917](https://arxiv.org/abs/2101.09917)].

- [15] D.-E. Liebscher, W. Priester and J. Hoell, *Lyman-alpha forest and the evolution of the universe.*, *Astronomische Nachrichten* **313** (Sept., 1992) 265–273.
- [16] D. Weinberg, *Measuring Cosmological Parameters with the Lyman-alpha Forest*, in *APS April Meeting Abstracts*, APS Meeting Abstracts, p. 8WK.05, Apr., 1998.
- [17] U. Seljak, P. McDonald and A. Makarov, *Cosmological constraints from the cosmic microwave background and Lyman α forest revisited*, *MNRAS* **342** (July, 2003) L79–L84, [[astro-ph/0302571](#)].
- [18] R. Mandelbaum, P. McDonald, U. Seljak and R. Cen, *Precision cosmology from the Lyman α forest: power spectrum and bispectrum*, *MNRAS* **344** (Sept., 2003) 776–788, [[astro-ph/0302112](#)].
- [19] S. Bird, M. Fernandez, M.-F. Ho, M. Qezlou, R. Monadi, Y. Ni et al., *Priya: A new suite of lyman-alpha forest simulations for cosmology*, 2023.
- [20] H. Tohfa, S. Bird, M.-F. Ho, M. Qezlou and M. Ferandez, *Forecast cosmological constraints with the 1d wavelet scattering transform and the lyman- α forest*, 2023.
- [21] N. K. Khan, G. Kulkarni, J. S. Bolton, M. G. Haehnelt, V. Iršič, E. Puchwein et al., *Particle initialization effects on Lyman- α forest statistics in cosmological SPH simulations*, *arXiv e-prints* (Oct., 2023) [arXiv:2310.07767](#), [[2310.07767](#)].
- [22] J. Schaye, T. Theuns, A. Leonard and G. Efstathiou, *Measuring the temperature of the intergalactic medium*, in *Building Galaxies; from the Primordial Universe to the Present* (F. Hammer, T. X. Thuan, V. Cayatte, B. Guiderdoni and J. T. Thanh Van, eds.), p. 455, Jan., 2000. [astro-ph/9905364](#). DOI.
- [23] J. S. Bolton, M. G. Haehnelt, M. Viel and V. Springel, *The lyman α forest opacity and the metagalactic hydrogen ionization rate at $z \sim 2 - 4$* , *Monthly Notices of the Royal Astronomical Society* **357** (mar, 2005) 1178–1188.
- [24] P. Gaikwad, M. Rauch, M. G. Haehnelt, E. Puchwein, J. S. Bolton, L. C. Keating et al., *Probing the thermal state of the intergalactic medium at $z > 5$ with the transmission spikes in high-resolution Ly α forest spectra*, *MNRAS* **494** (June, 2020) 5091–5109, [[2001.10018](#)].
- [25] P. Gaikwad, R. Srianand, M. G. Haehnelt and T. R. Choudhury, *A consistent and robust measurement of the thermal state of the IGM at $2 \leq z \leq 4$ from a large sample of ly α forest spectra: evidence for late and rapid he reionization*, *Monthly Notices of the Royal Astronomical Society* **506** (jul, 2021) 4389–4412.
- [26] A. Font-Ribera, *Dark Energy with DESI*, in *42nd COSPAR Scientific Assembly*, vol. 42, pp. E1.1–15–18, July, 2018.
- [27] N. G. Karaçaylı, A. Font-Ribera and N. Padmanabhan, *Optimal 1D Ly α forest power spectrum estimation - I. DESI-lite spectra*, *MNRAS* **497** (Oct., 2020) 4742–4752, [[2008.06421](#)].
- [28] M. Walther, E. Armengaud, C. Ravoux, N. Palanque-Delabrouille, C. Yèche and Z. Lukić, *Simulating intergalactic gas for DESI-like small scale Lyman α forest observations*, *J. Cosmology Astropart. Phys.* **2021** (Apr., 2021) 059, [[2012.04008](#)].
- [29] Z. Ding, C.-H. Chuang, Y. Yu, L. H. Garrison, A. E. Bayer, Y. Feng et al., *The DESI N-body Simulation Project II: Suppressing Sample Variance with Fast Simulations*, *arXiv e-prints* (Feb., 2022) [arXiv:2202.06074](#), [[2202.06074](#)].
- [30] S. Gontcho A Gontcho and I. Pérez Ràfols, *First measurements of Lyman alpha correlations from DESI*, in *APS April Meeting Abstracts*, vol. 2022 of *APS Meeting Abstracts*, p. H13.005, Apr., 2022.
- [31] G. Dalton, S. C. Trager, D. C. Abrams, D. Carter, P. Bonifacio, J. A. L. Aguerri et al., *WEAVE: the next generation wide-field spectroscopy facility for the William Herschel Telescope*, in *Ground-based and Airborne Instrumentation for Astronomy IV* (I. S. McLean,

- S. K. Ramsay and H. Takami, eds.), vol. 8446 of *Society of Photo-Optical Instrumentation Engineers (SPIE) Conference Series*, p. 84460P, Sept., 2012. DOI.
- [32] K. Kraljic, C. Laigle, C. Pichon, S. Peirani, S. Codis, J. Shim et al., *Forecasts for WEAVE-QSO: 3D clustering and connectivity of critical points with Lyman- α tomography*, *arXiv e-prints* (Jan., 2022) arXiv:2201.02606, [2201.02606].
- [33] B. Arya, T. R. Choudhury, A. Paranjape and P. Gaikwad, *Lognormal seminumerical simulations of the lyman α forest: comparison with full hydrodynamic simulations*, *Monthly Notices of the Royal Astronomical Society* **520** (feb, 2023) 4023–4036.
- [34] M. M. Ivanov, *Don't miss the forest for the trees: the lyman alpha forest power spectrum in effective field theory*, 2023.
- [35] C. Jacobus, P. Harrington and Z. Lukić, *Reconstructing lyman- α fields from low-resolution hydrodynamical simulations with deep learning*, 2023.
- [36] G. Rossi, N. Palanque-Delabrouille, C. Yeche, A. Borde, J. Rich, M. Viel et al., *Neutrino Masses, Cosmological Parameters and Dark Energy from the Transmitted Flux in the Lyman-alpha Forest*, in *American Astronomical Society Meeting Abstracts #221*, vol. 221 of *American Astronomical Society Meeting Abstracts*, p. 323.04, Jan., 2013.
- [37] A. Borde, N. Palanque-Delabrouille, G. Rossi, M. Viel, J. S. Bolton, C. Yè che et al., *New approach for precise computation of lyman- α forest power spectrum with hydrodynamical simulations*, *Journal of Cosmology and Astroparticle Physics* **2014** (jul, 2014) 005–005.
- [38] F. Nasir, J. S. Bolton and G. D. Becker, *Inferring the IGM thermal history during reionization with the lyman α forest power spectrum at redshift $z \simeq 5$* , *Monthly Notices of the Royal Astronomical Society* **463** (aug, 2016) 2335–2347.
- [39] B. Villaseñor, B. Robertson, P. Madau and E. Schneider, *New constraints on warm dark matter from the lyman- α forest power spectrum*, *Physical Review D* **108** (jul, 2023) .
- [40] V. Iršič, M. Viel, M. G. Haehnelt, J. S. Bolton, M. Molaro, E. Puchwein et al., *Unveiling Dark Matter free-streaming at the smallest scales with high redshift Lyman-alpha forest*, *arXiv e-prints* (Sept., 2023) arXiv:2309.04533, [2309.04533].
- [41] L. Cabayol-Garcia, J. Chaves-Montero, A. Font-Ribera and C. Pedersen, *A neural network emulator for the lyman- α 1d flux power spectrum*, 2023.
- [42] Planck Collaboration, P. A. R. Ade, N. Aghanim, C. Armitage-Caplan, M. Arnaud, M. Ashdown et al., *Planck 2013 results. XVI. Cosmological parameters*, *A&A* **571** (Nov., 2014) A16, [1303.5076].
- [43] A. Lewis and A. Challinor, “CAMB: Code for Anisotropies in the Microwave Background.” Astrophysics Source Code Library, record ascl:1102.026, Feb., 2011.
- [44] J. S. Bolton, E. Puchwein, D. Sijacki, M. G. Haehnelt, T.-S. Kim, A. Meiksin et al., *The Sherwood simulation suite: overview and data comparisons with the Lyman α forest at redshifts $2 \leq z \leq 5$* , *MNRAS* **464** (Jan., 2017) 897–914, [1605.03462].
- [45] G. Kulkarni, J. F. Hennawi, J. Oñorbe, A. Rorai and V. Springel, *CHARACTERIZING THE PRESSURE SMOOTHING SCALE OF THE INTERGALACTIC MEDIUM*, *The Astrophysical Journal* **812** (oct, 2015) 30.
- [46] A. Rorai, G. D. Becker, M. G. Haehnelt, R. F. Carswell, J. S. Bolton, S. Cristiani et al., *Exploring the thermal state of the low-density intergalactic medium at $z = 3$ with an ultrahigh signal-to-noise QSO spectrum*, *MNRAS* **466** (Apr., 2017) 2690–2709, [1611.03805].
- [47] T. R. Choudhury, R. Srianand and T. Padmanabhan, *Semianalytic Approach to Understanding the Distribution of Neutral Hydrogen in the Universe: Comparison of Simulations with Observations*, *ApJ* **559** (Sept., 2001) 29–40, [astro-ph/0012498].

- [48] H. Bi, *Lyman-Alpha Absorption Spectrum of the Primordial Intergalactic Medium*, *ApJ* **405** (Mar., 1993) 479.
- [49] V. Springel, *The cosmological simulation code gadget-2*, *Monthly Notices of the Royal Astronomical Society* **364** (dec, 2005) 1105–1134.
- [50] A. Lewis and S. Bridle, *Cosmological parameters from CMB and other data: A monte carlo approach*, *Physical Review D* **66** (nov, 2002) .
- [51] A. Lewis, *Efficient sampling of fast and slow cosmological parameters*, *Physical Review D* **87** (may, 2013) .
- [52] J. Torrado and A. Lewis, *Cobaya: code for bayesian analysis of hierarchical physical models*, *Journal of Cosmology and Astroparticle Physics* **2021** (may, 2021) 057.
- [53] A. Gelman and D. B. Rubin, *Inference from Iterative Simulation Using Multiple Sequences*, *Statistical Science* **7** (Jan., 1992) 457–472.
- [54] J. Schaye, *Explaining the Lyman-alpha forest*, *arXiv e-prints* (Dec., 2001) astro-ph/0112022, [[astro-ph/0112022](#)].
- [55] D. J. Eisenstein and W. Hu, *Baryonic features in the matter transfer function*, *The Astrophysical Journal* **496** (apr, 1998) 605–614.
- [56] P. Petitjean, J. P. Mueket and R. E. Kates, *The Ly α forest at low redshift: tracing the dark matter filaments.*, *A&A* **295** (Mar., 1995) L9–L12, [[astro-ph/9502100](#)].
- [57] R. A. C. Croft, D. H. Weinberg, N. Katz and L. Hernquist, *Cosmology from the structure of the ly α forest*, in *Large Scale Structure: Tracks and Traces* (V. Mueller, S. Gottloeber, J. P. Muecket and J. Wambsganss, eds.), pp. 69–75, Jan., 1998. [astro-ph/9801255](#).
- [58] M. Viel and M. G. Haehnelt, *Cosmological and astrophysical parameters from the Sloan Digital Sky Survey flux power spectrum and hydrodynamical simulations of the Lyman α forest*, *MNRAS* **365** (Jan., 2006) 231–244, [[astro-ph/0508177](#)].
- [59] S. Peirani, D. H. Weinberg, S. Colombi, J. Blaizot, Y. Dubois and C. Pichon, *LyMAS: Predicting Large-scale Ly α Forest Statistics from the Dark Matter Density Field*, *ApJ* **784** (Mar., 2014) 11, [[1306.1533](#)].
- [60] S. Peirani, S. Prunet, S. Colombi, C. Pichon, D. H. Weinberg, C. Laigle et al., *LyMAS reloaded: improving the predictions of the large-scale Lyman- α forest statistics from dark matter density and velocity fields*, *arXiv e-prints* (Apr., 2022) arXiv:2204.06365, [[2204.06365](#)].
- [61] F. Sinigaglia, F.-S. Kitaura, A. Balaguera-Antolínez, I. Shimizu, K. Nagamine, M. Sánchez-Benavente et al., *Mapping the three-dimensional ly α forest large-scale structure in real and redshift space*, *The Astrophysical Journal* **927** (mar, 2022) 230.
- [62] C. Pedersen, A. Font-Ribera, K. K. Rogers, P. McDonald, H. V. Peiris, A. Pontzen et al., *An emulator for the lyman- α forest in beyond- Λ CDM cosmologies*, *Journal of Cosmology and Astroparticle Physics* **2021** (may, 2021) 033.
- [63] B. Arya, A. Paranjape and T. R. Choudhury, *Covariance matrices for the lyman- α forest using the lognormal approximation*, 2023.